SJER Scientific Journal of Engineering Research

futuristech PT. Teknologi Futuristik Indonesia

Date of publication April 23, 2026, date of current version April 23, 2026.
e-ISSN: 3109-1725
Digital Object Identifier 10.64539/sjer.v2i2.2026.459

Article

Aerodynamic Optimization of Horizontal Axis Wind Turbine Blades Using Winglet and Spoiler Add-Ons: A CFD Study

Oluwaseyi Omotayo Alabi[1,*], Adeoti Oyegbori Laoye[1], Saidat Abisoye Salisu[1]

[1] Department of Mechanical Engineering, Lead City University, Ibadan 200255, Nigeria; e-mail: alabi.oluwaseyi@lcu.edu.ng (O. O. Alabi).
* Correspondence

The authors received no financial support for the research, authorship, and/or publication of this article.

Abstract: The aerodynamic performance of wind turbine blades plays a critical role in maximizing energy generation and overall system efficiency, making it a key consideration in modern renewable energy design. Despite extensive research on blade optimization, there remains a notable gap in understanding the combined effects of spoiler and winglet geometries, particularly their size and orientation on aerodynamic efficiency under low wind speed conditions. This study aims to address this gap by conducting a comprehensive numerical investigation into the influence of spoiler and winglet configurations on wind turbine performance. Computational Fluid Dynamics (CFD) simulations were performed using COMSOL Multiphysics, with the k-ε turbulence model employed to accurately capture turbulent flow behavior. A detailed parametric analysis was carried out, considering winglet height (4%–13% of blade radius), cant angle (20°–90°), twist angle (−2° to 12°), and tip speed ratio (0.02–1.12) at a wind velocity of 3 m/s. The results reveal that optimal combinations of spoiler and winglet parameters significantly enhance aerodynamic efficiency. The study identifies specific design ranges that maximize power output, achieving a peak aerodynamic power of 62.8 W. Although the addition of these aerodynamic devices increases the inertia of the turbine, the system performance improves, with an observed increase in output power of approximately 12%. These findings provide valuable insights for the design and optimization of wind turbine blades, particularly for low wind speed applications.

Keywords: Computational Fluid Dynamics (CFD), Add-on, Power output, Twist angle, Cant angle, Tip speed ratio.

1. Introduction

Some issues attributed to conventional power generation are related to high cost, environmental degradation, and adverse effects on the economy hence many countries are moving to different forms of alternative energy sources for energy generation [1]. Movement of solid bodies such as airfoils, through fluid stream, produces aerodynamic forces. Airfoil is a streamlined shape, capable of generating more lift than drag [2]. A major challenge in the efficient utilization of resources, with a focus on renewable sources. Wind turbines harness the kinetic energy of moving air, converting it to mechanical power via aerodynamic forces. This mechanical power is then transformed into electrical power through a generator, enabling it to be utilized for various applications [3]. To maximize the power output of wind turbines, enhancing their power coefficient is critical, necessitating the development of novel designs with superior power performance. This is a multifaceted engineering endeavor with significant potential benefits. In light of the environmental and supply concerns associated with conventional fossil fuels, the pursuit of clean and sustainable energy sources is of paramount importance [4], [5]. Among the most promising options is wind energy, which is projected to contribute significantly to the global electricity supply in the coming years. Numerous studies [6] underscore the potential of wind power to mitigate environmental impacts and diversify energy sources. According to [7], [8], wind energy is expected to generate up to 20% of the world's electricity by 2030.

From vortices to turbulence, the airflow around a

HAWT blade is a symphony of complex aerodynamic phenomena, captivating the curiosity of many researchers. Through intense analysis, these investigators seek to unravel the intricacies of how blades extract kinetic energy from wind turbines [9]. The interplay of eddies and turbulence in the blade's wake is a stunning manifestation of nature's fluid dynamics, inspiring awe and admiration in those who study it. Investigating these phenomena in an experimental setting demands precise and delicate instrumentation, capable of capturing the minutiae of the blade's aerodynamic properties. To capture these subtleties, researchers must utilize cutting-edge sensors, engineered with extraordinary sensitivity and accuracy [10]. In the pursuit of aerodynamic enlightenment, numerical simulations have emerged as a worthy contender, offering a compelling alternative to experimental investigations. Among efficient tools for deciphering aerodynamic effects are Computational Fluid Dynamics (CFD) modules and Blade Element Momentum (BEM) method, revered for their accuracy and reliability. The BEM method slices and dices the blade into a series of sections, calculating the lift and drag forces at each section based on the properties of the airfoil shapes that make up the blade. These airfoils, the unsung heroes of the blade, generate lift and drag through subtle pressure variations on their surfaces [8]. The components responsible for extracting energy from the wind in a horizontal-axis wind turbine are the airfoils that make up the blades. These airfoils, which can be conceptualized as a series of two-dimensional aerodynamic profiles, utilize the pressure differences between their upper and lower surfaces to generate lift and drag forces, which are subsequently converted into usable electrical energy through the mechanical rotation of the turbine [8]. Although BEM offers a straightforward approach to analyzing the performance of wind turbines, its limitations become apparent when applied to high wind speeds [8], [11]. At higher velocities, the model's predictions of torque output become increasingly inaccurate due to the effects of tip losses, which cannot be accounted for using the BEM approach. However, various correction factors have been developed to compensate for tip losses, improving the predictive capabilities of BEM under high wind speed conditions [12], [13].

CFD (Computational Fluid Dynamics) emerged as a prominent tool in simulating fluid dynamics problems, including those involving wind turbines. Its ability to accurately capture intricate fluid-flow patterns around the turbine, particularly, tip vortices, has made it a valuable resource in the analysis of turbine performance [14]. In recent years, numerous studies have focused on using CFD to investigate the aerodynamic behavior of turbine blades, with a particular emphasis on the impact of tip vortices on lift and drag forces. One innovative solution for mitigating the adverse effects of tip vortices is the winglet, which can be attached to the tip of the blade [15]. Its primary function is to redirect the tip vortices away from the plane of rotation, thereby reducing their impact on the lift and drag forces on the blade [16]. Furthermore, the winglet can enhance the blade's span-wise flow, thereby reducing downwash.

Khalafallah et al. [17], explored numerical methods to investigate the effects of various winglet parameters on the aerodynamic performance of a wind turbine. Through their analysis, they concluded that the addition of a winglet to a conventional blade resulted in a 2.8% boost in power output, primarily due to an increase in the winglet height by 4%R. The researchers also utilized Computational Fluid Dynamics modules to examine different winglets of diverse twists and cambers configurations, while maintaining a fixed height of 1.5%R and a cant angle of 90°. They observed that for wind speeds above 6 m/s, the power output increased by a range of 0.6% to 1.4%, which highlights the significant impact of winglet design on turbine performance.

Mourad et al. [18], investigated performance of blades of wind turbine winglet taking two key parameters into consideration by providing winglet to wind turbine blade of 20% which increased output power of winglet height 4% of rotor radius at a cant-angle of 45°. The addition of a winglet to blade increases start-torque for low tip speed-ratio. Power coefficient was noticed to be increased by addition of double winglets to smaller installation angles to resulting in to increase of the circumferential component of the lift [19].

Reddy et al. [19], focused on the impacts of winglets on the performance of wind turbine blades by considering winglet height and cant angle. The findings revealed that the addition of a winglet to straight blade led to a remarkable 20% boost in power output, with an optimal height of 4% of rotor radius and cant-angle of 45°. Another CFD analysis by [8], [20], is concerned with enhancing rotor performance by scrutinizing the influence of winglet height and radius of curvature. Results showed a 25% increase in winglet height that led to a 1.7% uptick in power output, indicating the substantial impact of these parameters on the overall performance of the rotor.

Verma et al. [21], used experimental and numerical analysis to examine the effects of different winglet configurations on power coefficient. The findings revealed that an upwind winglet configuration led to a 6.67% increase in power coefficient, while a downwind winglet resulted in an 8.89% dropped, highlighting the significant impact of winglet placement on rotor performance. [22] worked on numerical analysis to pinpoint the optimal aerodynamic efficiency of turbine rotors with winglets. Their findings indicated that downwind winglets (bending towards the suction side) offered greater efficiency than upwind winglets (bending towards the pressure side), for winglets of equal length. Turbines are essential components of many industries, as they are used to produce

electric power through gas or steam turbines. As with any rotating machine, regular maintenance is essential to ensure maximum reliability. This includes scheduled inspections, repairs, and replacement of defective parts. Through careful maintenance, turbines can operate at peak efficiency for years to come [23]-[25].

The main limitation of this study is that the results obtained from the numerical investigation of the aerodynamic behavior of add-on devices for horizontal axis wind turbines (HAWT) are based on simulations and may not accurately represent real-world conditions. To improve the performance of horizontal-axis wind turbine blades, it is important to explore new designs for add-on elements. The size and orientation of add-ons can have a significant impact on the aerodynamic behavior of blades, which in turn affects the overall energy production. This paper aims to investigate how the size and orientation of add-ons affect aerodynamic performance, to identify optimal placements and sizes that maximize wind energy capture. In addition, the paper considers the potential of active surfaces or shape-shifting add-ons that can dynamically adjust to changing wind conditions in real time. This work used the COMSOL Multiphysics software to carry out numerical simulations that probe the aerodynamic characteristics of horizontal axis wind turbine blades equipped with spoilers and winglets. The accuracy of the simulations was verified by comparing them with previous work by Khalafallah et al, 2019 [17], with the resulting error percentages within acceptable limits. The simulations were then used to examine the performance of blades with various parameters and configurations, including those with winglets and spoilers. This allowed for an in-depth analysis of how these add-on elements affect the aerodynamic performance of the blades.

This study lies in its integrated aerodynamic optimization approach that simultaneously investigates the combined effects of winglet and spoiler add-ons on horizontal axis wind turbine (HAWT) blades using high-fidelity CFD analysis. Unlike conventional studies that examine either winglets *or* spoilers independently, this work introduces a hybrid aerodynamic control strategy, where both devices are applied and optimized together to enhance blade performance. This dual-add-on configuration enables a more comprehensive control of flow behavior, targeting both tip vortex reduction (via winglets) and flow separation control (via spoilers) within a unified framework. A key innovative aspect is the systematic parametric investigation of multiple design variables, including spoiler deflection angles, winglet geometries, and blade twist configurations, across a range of tip speed ratios. This allows for the identification of optimal interaction effects between add-ons rather than isolated performance improvements.

This paper is organized as follows. Section 2 presents the methodology, Blade geometry, and computational Fluid Dynamics analysis. Section 3 Results and discussion. Section 4 presents the conclusion and future works.

2. Methodology

2.1. Blade Parameters and Geometry

Winglets, also known as wing tip devices, or add-on are small appendages attached to the tip of a blade. These devices are designed to reduce the induced drag, which is generated by the turbulent airflow around the blade. The winglet achieves this by redirecting the airflow in a manner that mitigates the formation of vortices and improves the aerodynamic performance of the blade [6], [26]. While winglets may improve lift-to-drag ratio, they also introduce additional drag due to their size and surface area. Critical parameters that govern winglet design include, height, twist-angle, cant-angle, and tip speed-ratio (see Figure 1a). Geometry of a winglet-equipped blade is depicted in Figure 1b, showcasing aerodynamic spoiler integration.

This study selected four key parameters as winglet height, twist-angle, cant-angle, tip speed-ratio. To explore the impact of these parameters on the winglet design, 20 different designs were created, each with varying values for the four parameters. It's worth noting that previous studies have only investigated winglets bent towards the suction or pressure side, but in this study, we're focusing on the add-on bending towards the pressure side, as illustrated in Figure 1b. As indicated in Table 1, the twist angle is kept constant from winglet 1 to 5 while other three parameters (cant angle, winglet height and tips speed ratio), are varies from 6% to 13%, 20^0 to 90^0, and 0.02 to 0.11 respectively. The twist angle is kept constant from winglet 6 to 10 while other three parameters (cant-angle, height of winglet and tip-speed ratio), are varies from 4% to12%, 20^0 to 90^0, and 0.12 to 0.5 respectively. Winglet design of 11 to 15 were investigated with height and twist-angle, while cant-angle, tip-speed ratio varied from 20° to 90°, 0.57 to 0.65 respectively. Also, design of winglet from 16 to 20 were done with cant-angle and tip-speed ratio varied from 20° to 90°, 0.69 to 1.2 respectively.

2.2. Computational Fluid Dynamics (CFD) Modeling

CFD model of wind turbine blade was created with COMSOL Multiphysics. Due to turbine's asymmetry, a single blade with an angle of 115^0 was modeled, representing three blades. Front and top planes were set as inlets of velocity, where air flows freely. Rear plane was designated as pressure outlet, allowing air to exit the system. Once the geometry was constructed, it was crucial to assign the fluid volumes and discretize them through meshing. There are various meshing techniques available, including coarse, fine, and normal elements. For this study, an extremely fine mesh was employed 80652 degree of freedom and 123136 DOFs to capture the flow details accurately. Figure 2 shows the mesh geometry with special attention to inflation layer at the wall.

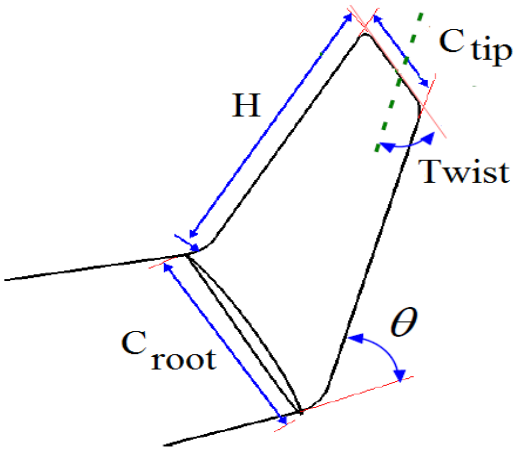

(a)

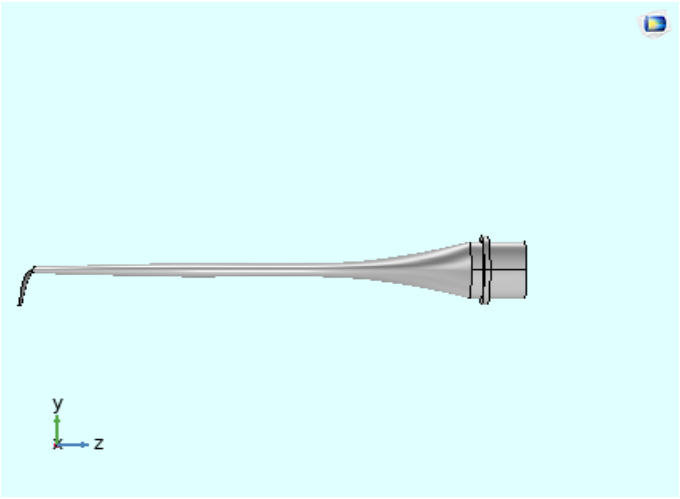

(b)

Figure 1. (a) Add-on parameters [7], (b) Blade geometry with add-on.

Table 1. Parameter variation of add-on designs.

Add-on	Height (%R)	Cant Angle (θ)	Twist angle (β)	Tip speed ratio (λ)
1	13	20	-2	0.02
2	12	40		0.06
3	10	60		0.076
4	8	80		0.09
5	6	90		0.11
6	12	20	4	0.12
7	9	40		0.28
8	8	60		0.34
9	6	80		0.42
10	4	90		0.5
11	8	20	10	0.57
12		40		0.59
13		60		0.6
14		80		0.62
15		90		0.65
16	8	20	12	0.69
17		40		0.72
18		60		0.91
19		80		1.0
20		90		1.2

2.3. Turbulence model

Turbulence is a ubiquitous phenomenon in fluid flows, arising from the interplay between viscous boundary effects and fluid separation from surfaces. The steady-state behaviour of turbulent flows can be predicted using Reynolds Averaged Navier-Stokes (RANS) equations, which account for spatial and temporal variations of flow properties [8]. By solving these equations, valuable insights into the flow characteristics can be obtained. The RANS (Reynolds Averaged Navier-Stokes) model is widely recognized for solving the Navier-Stokes equations, which describe the behavior of fluid flow [12], [16]. By replacing the instantaneous velocity field with an averaged one, RANS offers an efficient approach for capturing the dominant flow characteristics without requiring the full resolution of the Navier-Stokes equations, making it a popular choice among engineers and scientists. RANS equations are commonly solved with a variety of turbulence models, with the k-ε and k-ω SST models being popular choices for wind energy applications. The k-ε model estimates the eddy viscosity by solving for the turbulent dissipation rate and kinetic energy, also it can be applied to a wide range of flow conditions, from laminar to turbulent flows while the k-ω SST model incorporates additional terms to better capture the effects of rotation and streamline curvature. Both models enable more accurate solutions for complex flow phenomena in wind energy systems. SST turbulence models display a distinct edge over traditional RANS models in instances of transition-to-turbulence, in which flow separation and stall are wont to transpire. Within a milieu characterized by low Reynolds numbers, the venerable k-ε turbulence model, is known for its proficiency in discerning the intricacies of boundary layer behaviour. The k-ε turbulence model is a two-equation model that uses the turbulence kinetic energy k and the specific rate of dissipation ε to predict turbulent flow behaviour. Its primary advantage lies in its ability to accurately represent the intricacies of boundary layer flow, particularly in the presence of adverse pressure gradients and flow separation.

2.4. Governing Equation

For a turbine operating under constant wind speed, the power coefficient;

$$C_P = \frac{2T\omega}{\rho\pi R^2 U_\infty^3} \quad [17] \tag{1}$$

where T is the torque generated by the rotor, ω is the rotation speed, ρ is the air Density while the coefficient of thrust and tip speed ratio (TSR) = λ are;

$$C_T = \frac{2F_D}{\rho\pi R^2 U_\infty^2} \quad [17] \tag{2}$$

Figure 2. Meshing configuration around the blade.

where F_D is the drag force.

$$\lambda = \frac{\omega R}{U_\infty} \tag{3}$$

where R is the Diameter of the rotor.

The axial thrust exerted on the wind turbine rotor by the flow field can be computed using the momentum theorem, which requires an evaluation of the rate of change in momentum.

$$T = \rho A U_d (U_\infty - U_w) \tag{4}$$

where ρ is the air density, A is the rotor swept area, U_∞ is the wind speed, U_w is the velocity at the infinity wind turbine downstream, U_d is the axial velocity of fluid passing through the wind rotor.

The pressure coefficient is given by:

$$C_{pressure} = \frac{2(P - P_\infty)}{\rho(U_\infty^2 + (\omega r)^2)} \tag{5}$$

where, P is static pressure
P_∞ is free-stream static pressure
ω is angular velocity
r is radial distance from the hub Centre to the blade section

$$\rho \frac{\partial u}{\partial t} + \rho(u.\nabla)u = \nabla.[p\mathrm{I} + \mathbf{K}] + F \tag{6}$$

The equation can be written as:

$$\rho \frac{\partial u}{\partial t} + \nabla.(\rho u u) = \nabla.[p\mathrm{I} + \mathbf{K}] + F \tag{7}$$

$$\mathrm{K} = \frac{\tau}{\rho} = (\mu + \mu_T)(\nabla u + (\nabla u)^T) - \frac{2}{3}(\mu + \mu_T)(\nabla.u)\mathrm{I} - \frac{2}{3}\rho\kappa\mathrm{I} \tag{8}$$

$$\tau = \mu(\nabla u + (\nabla u)^T - \mathrm{pI} \tag{9}$$

Then, the continuity equation for conservation of mass and momentum equation can be written in vectorial form:

$$\frac{\partial \rho}{\partial t} + \nabla.\rho u = 0 \tag{10}$$

$$\nabla.(\rho u) = 0 \tag{11}$$

$$\frac{\partial}{\partial t}\begin{pmatrix}\rho u \\ \rho v\end{pmatrix} + \rho\begin{pmatrix}\frac{\partial u}{\partial x} + \frac{\partial u}{\partial y} \\ \frac{\partial v}{\partial x} + \frac{\partial v}{\partial y}\end{pmatrix} = 0 \tag{12}$$

The momentum equation is:

From equation 6 substitute for shear for tensor viscous effect K, then equation become equation 13 for overall momentum equation:

$$\frac{\partial}{\partial t}(\rho u) + \nabla.(\rho u u) = \nabla.(\mu(\nabla u + \nabla u^T)) - \nabla \mathrm{pI} + F \tag{13}$$

$$\frac{\partial}{\partial t}(\rho u) + \nabla.(\rho u u) = \nabla.(\tau - \mathrm{pI}) \tag{14}$$

where, the stress tensor τ for compressible fluid is given in terms of the deformation rates as:

$$\tau = \mu(\nabla u + (\nabla u)^T \tag{15}$$

The momentum Equation 13 can be written in matrix for as:

$$\begin{aligned}\frac{\partial}{\partial t}\rho\begin{bmatrix}u \\ v\end{bmatrix} + \rho\begin{bmatrix}uu & uv \\ vu & vv\end{bmatrix}\begin{bmatrix}\nabla_x \\ \nabla_y\end{bmatrix} &= \begin{bmatrix}\mu\frac{\partial u}{\partial x} & \mu\frac{\partial u}{\partial y} \\ \mu\frac{\partial v}{\partial x} & \mu\frac{\partial v}{\partial y}\end{bmatrix}\begin{bmatrix}\nabla_x \\ \nabla_y\end{bmatrix} \\ &+ \begin{bmatrix}\mu\frac{\partial u}{\partial x} & \mu\frac{\partial v}{\partial x} \\ \mu\frac{\partial u}{\partial y} & \mu\frac{\partial v}{\partial y}\end{bmatrix}\begin{bmatrix}\nabla_x \\ \nabla_y\end{bmatrix} \\ &- \begin{bmatrix}p & \\ & p\end{bmatrix}\begin{bmatrix}\nabla_x \\ \nabla_y\end{bmatrix} + \begin{bmatrix}F_x \\ F_y\end{bmatrix}\end{aligned} \tag{16}$$

Neglecting dissipation effects, the energy equation can be written in term of temperature T as:

$$\frac{\partial}{\partial t}(\rho c_p T) + \nabla.(\rho c_p u T) = \nabla.(\mathrm{K}\nabla \mathrm{T}) \tag{17}$$

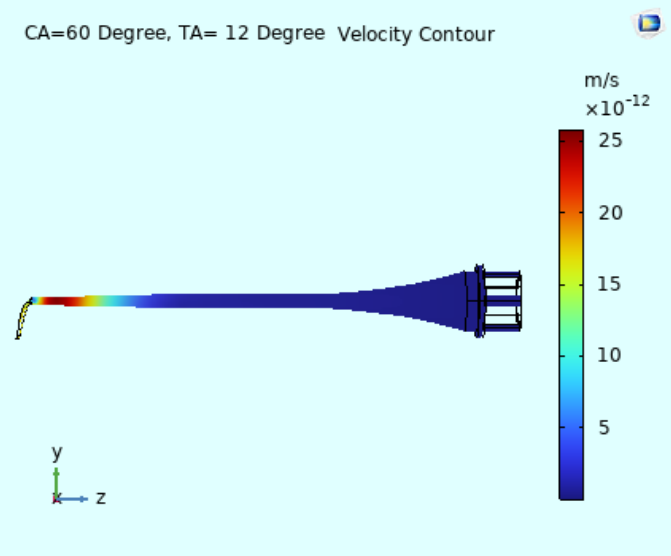

(a)

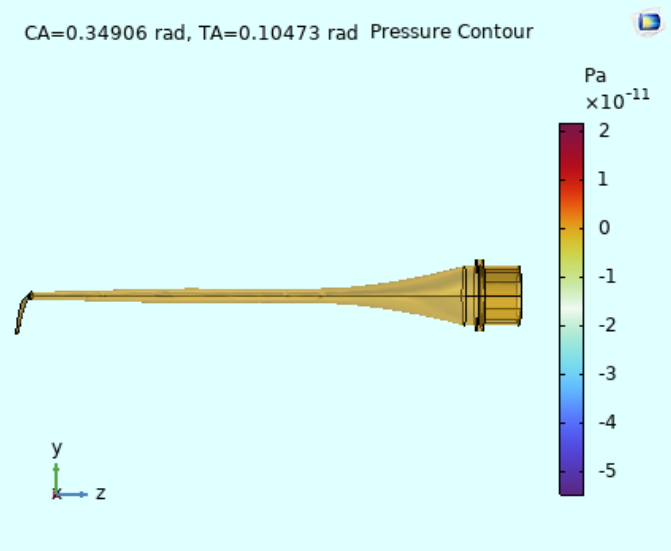

(b)

Figure 3. (a) Velocity contour, (b) Pressure contour.

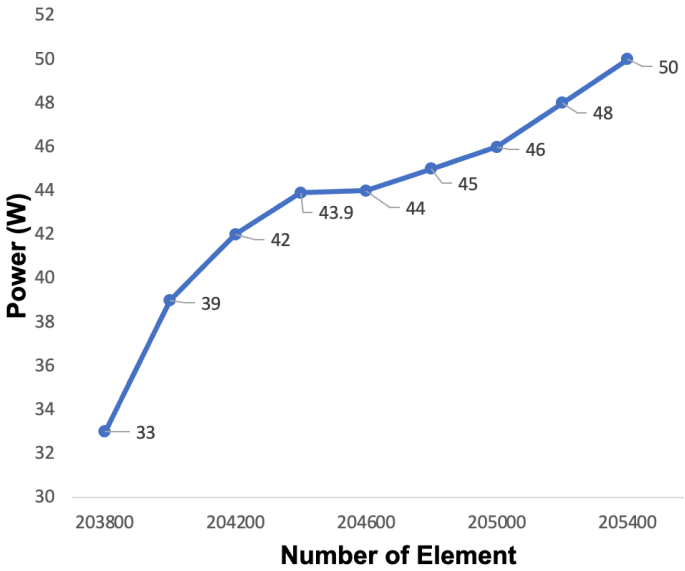

Figure 4. Grid sensitivity versus output power of turbine.

The RANS (Reynolds Averaged Navier-Stokes) method will be utilized in this research to accurately predict the system's performance within the design constraints. The underlying governing equations for the RANS method, which underpin the simulations, are as follows.

Reynolds Averaged Navier-Stokes equations:

$$\frac{dp}{dt} = -\frac{\partial}{\partial x_i}(\rho \bar{u}_i) \tag{18}$$

$$\frac{\partial}{\partial x_j}(\rho \bar{u}_i \bar{u}_j) = -\frac{d\bar{p}}{dx_i} + \frac{\partial}{\partial x_j}[u(\frac{d\bar{u}_i}{dx_j} + \frac{d\bar{u}_j}{dx_i} - \frac{2}{3}\delta_{ij}\frac{\partial \bar{u}_n}{\partial x_n})] + \frac{\partial}{\partial x_j}(-\rho\overline{u'_i u'_j}) \tag{19}$$

$$\frac{\partial}{\partial t}(\rho \bar{u}_i) = 0 \tag{20}$$

In equations (18) to (20), ρ is the average density and p is the average pressure, while μ is the dynamic viscosity and $(-\rho\overline{u'_i u'_j})$ is the Reynold stress tensor. The Reynolds stresses in the Reynolds-averaged approach must be properly predicted for effective turbulence modeling. The Boussinesq hypothesis, which links the Reynolds stresses to mean velocity gradients, uses a similar methodology as shown in Equation (15).

$$(-\rho\overline{u'_i u'_j}) = -\frac{2}{3}(\rho k + \mu_t \frac{d\bar{u}_i}{dx_i})\delta_{ij} + \mu_t(\frac{d\bar{u}_i}{dx_j} + \frac{d\bar{u}_j}{dx_i}) \tag{21}$$

To effectively solve RANS equations, closure techniques are required, and this is accomplished by deriving additional transport equations for the turbulent viscosity μ_t and the turbulent kinetic energy k. The selection of the appropriate turbulence model is critical in determining the level of accuracy and robustness of the results, as it governs the characteristics of μ_t and k in the additional equations [27], [28].

3. Results and Discussion

Power generated by the blade can be calculated by applying equation (1). From the CFD analysis, torque on blade and output power were 0.345 Nm and 62W respectively. It is imperative to note that these values represent a significant amount of mechanical energy extracted from the fluid flow by the blade, highlighting the intricate relationship between the blade design and the fluid dynamics. Figure 3a and Figure 3b depict the velocity and pressure contours, respectively, revealing the impact of tip vortex on the rotor's performance. Figure 3b showcases the tip vortex core location through the telltale brown color, while the latter demonstrates the ability of the winglet-equipped blade to mitigate the vortex-effect by shifting core further from blade tip.

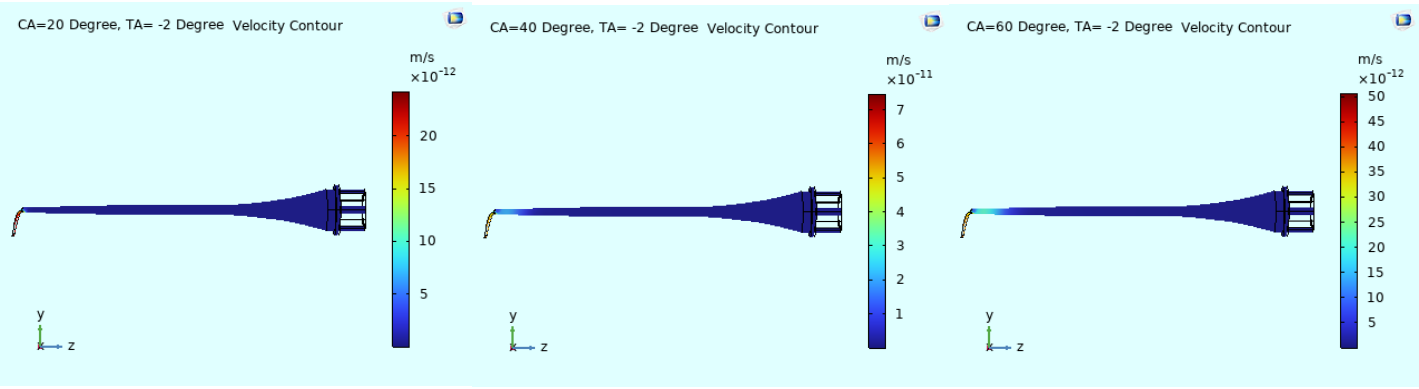

(a) *(b)* *(c)*

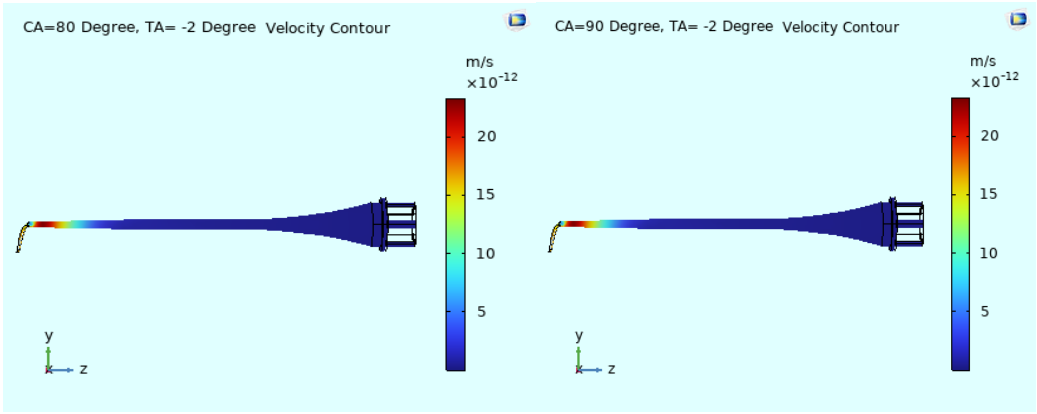

(d) *(e)*

Figure 5. Variation of cant angle θ at constant twist angle of β =-2^0.

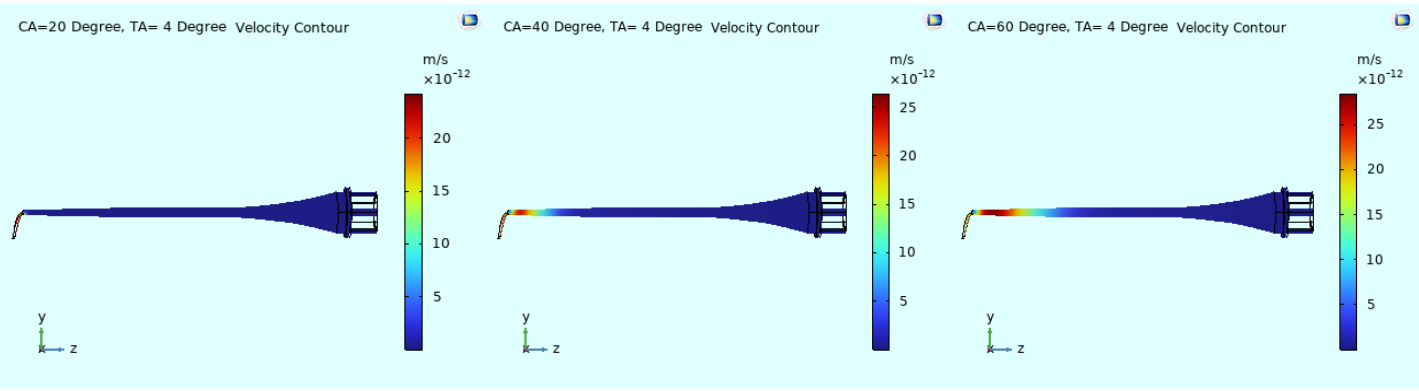

(a) *(b)* *(c)*

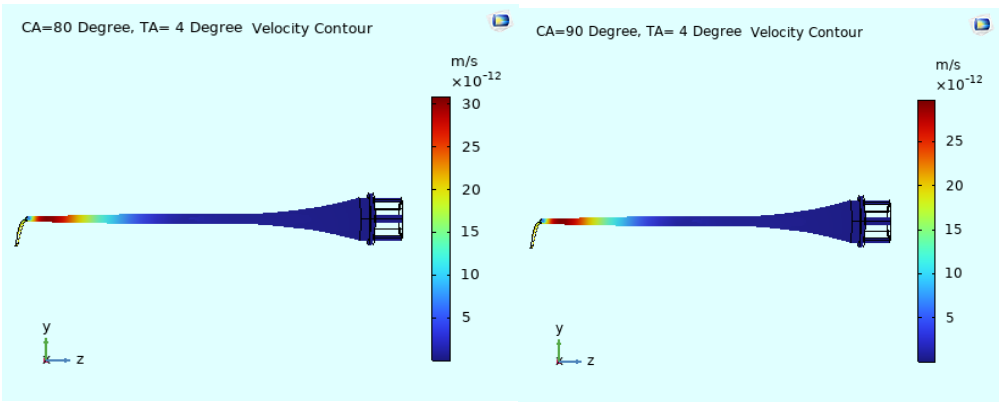

(d) *(e)*

Figure 6. Variation of cant angle θ at constant twist angle of β =4^0.

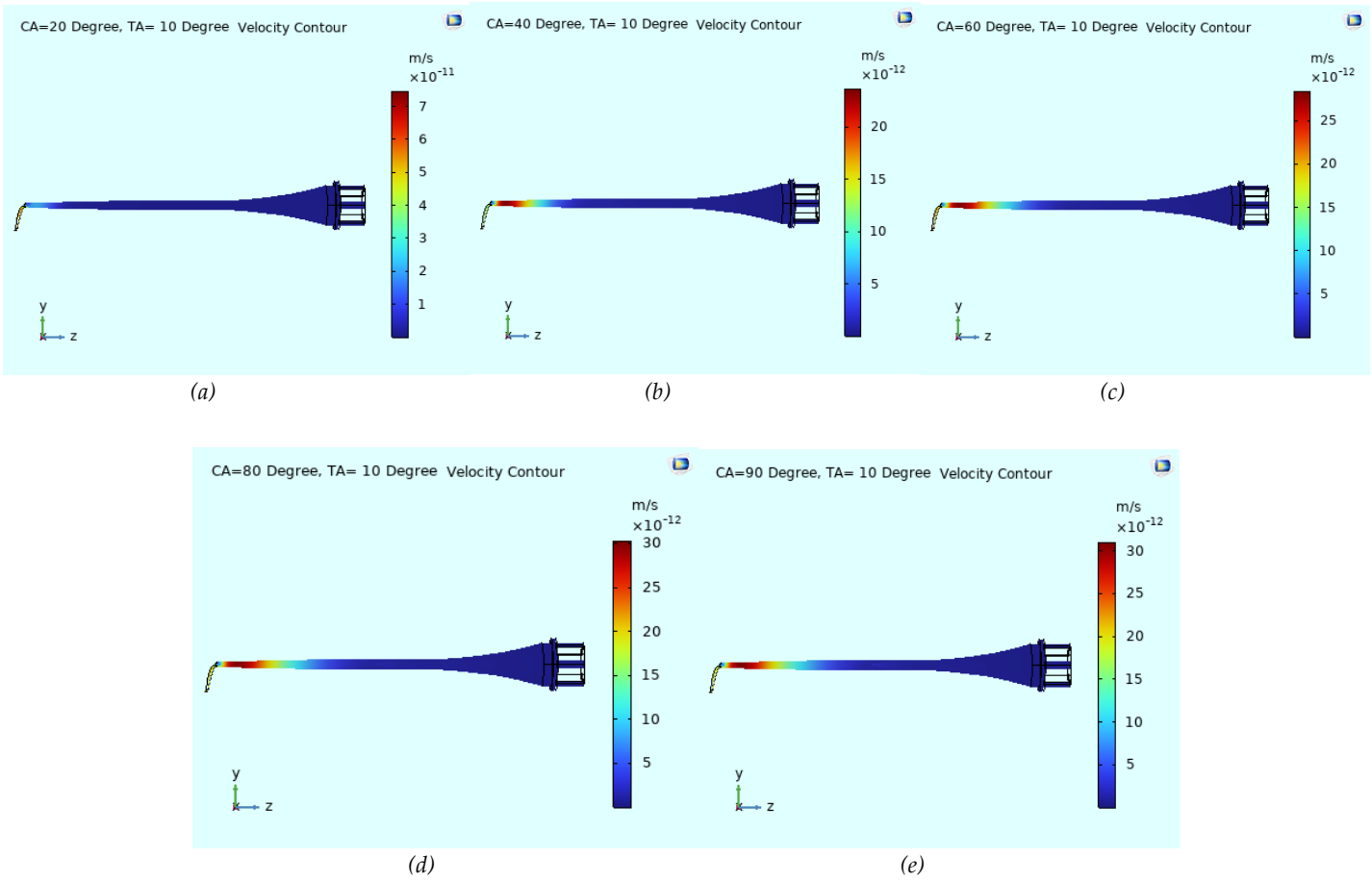

Figure 7. Variation of cant angle θ at constant twist angle of β =10^0.

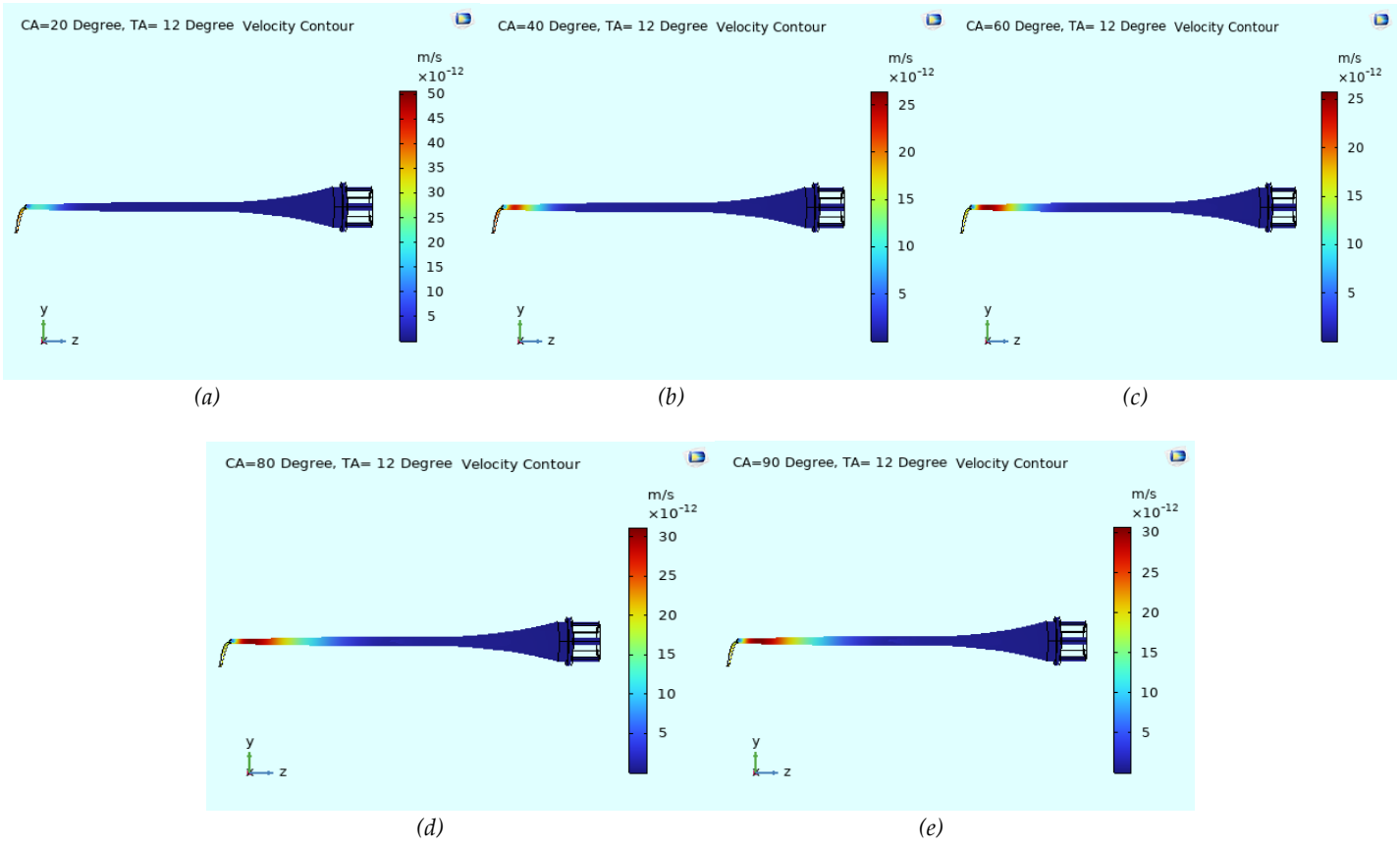

Figure 8. Variation of cant angle θ at constant twist angle of β =12^0.

Table 2. Result showing Power in variation of twist angle (β) at H = 8%R, λ = 0.6.

Add-On	Cant Angle (θ)	Twist angle (β)	Power (W)
1	20	-2	34.3
2	40		34.8
3	60		35.1
4	80		35
5	90		36.2
6	20	4	58.5
7	40		59.3
8	60		59.5
9	80		58.7
10	90		59.1
11	20	10	61.4
12	40		61.3
13	60		62.8
14	80		62.7
15	90		62.8
16	20	12	60.4
17	40		62.3
18	60		62.5
19	80		63.2
20	90		62.4

Figure 4 highlights the critical role of grid refinement in the accuracy of the CFD solution. The number of grid elements and their size have a direct impact on the simulation's accuracy and percentage error. To ensure the robustness of the results, this study underwent a grid independence analysis, which involves varying the number of grid elements to assess the convergence of the solution. Simulations were carried out for nine grids. In a rigorous grid independence study encompassing nine meshes, the power output results were presented in Figure 4. Notably, the mesh with 205400 elements yielded the most accurate power output, albeit at a steep computational cost. The results underscore the intricate relationship between mesh complexity and computational efficiency.

Twist and cant-angles affected the velocity contour by altering the flow over the blade and winglet. Twist angle influences angle of attack of winglet, which alters pressure distribution over the blade and winglet. This in-turn altered the velocity distribution and contour over the blade and winglet while cant-angle altered angle of winglet in relation to blade's longitudinal direction, which influences span-wise flow over the blade and winglet. This affects the velocity distribution and contour along the blade and winglet. Figures 5, 6, 7, and 8 presents the variation of cant angle at constant twist angle of -2° 4° 10° 12°. Upon inspecting Figures 7 and 8, the winglet's impact becomes quite obvious. These diagrams portray the velocity contour at constant angles of 10 and 12 degrees, respectively, where vortex core at winglet's tip is visibly weaker than on a conventional blade without a winglet Further analysis reveals that the vortex dissipates at a greater distance from the blade's tip when a winglet is incorporated, thereby affirming the favorable effect of this modification. Moreover, the angle of attack of the winglet is acutely influenced by the twist angle, which determines the angle at which the winglet intersects the incoming flow. Blade with add-on at cant-angle of 20°, 40°, 60°, 80°, 90° were investigated at winglet height, twist angle and tip speed ratio of 8%R, -2° 4° 10° 12°, and 0.6 respectively. (Table 2). Results indicated increase in power obtained with increase in twist- angle and cant-angle. Maximum power of 62.8 W occurred at cant-angle of 60° and twist angle of 10°. The power generated by the turbine hinges on a quartet of critical parameters: cant-angle, winglet height, twist angle and tip speed ratio.

Figure 9 succinctly summarizes the impact of these variables on turbine power at varying twist angles. A salient observation is the positive correlation between turbine power and tip speed ratio, while a converse relationship is apparent with respect to cant angle. Findings gives insights to intricate interplay in design parameters and impacts on turbine performance. This study examined the impact of tip speed-ratio and cant-angle on the aerodynamic performance of wind turbine blades. The results showed that both of these parameters can have a significant impact on blade performance, with different combinations of tip speed-ratio and cant-angle resulting in different levels of efficiency and energy output. Understanding the relationship between these parameters and blade performance is crucial for optimizing wind turbine design.

The figures demonstrate the variation of turbine output power with tip speed ratio (λ) for different spoiler/winglet orientation angles (θ) at two blade twist angles, $\beta = -2°$ and $\beta = 4°$, which is directly relevant to the aerodynamic optimization of horizontal axis wind turbine (HAWT) blades using add-on devices. At $\beta = -2°$ (Figure 9a), the generated power increases progressively with increasing tip speed ratio for all angular configurations, indicating that the aerodynamic performance of the blade improves as rotational speed becomes better matched to the incoming wind velocity. Among the tested cases, the $\theta = 20°$ configuration consistently produces the highest power output, reaching approximately 41 W at $\lambda = 0.11$, while the $\theta = 90°$ configuration gives the lowest performance throughout the operating range. This suggests that a moderate add-on orientation enhances the local airflow over the blade surface, delays boundary-layer separation, and reduces tip vortex losses, thereby improving lift generation. The lower performance at higher θ values may be associated with increased flow disturbance and drag penalties introduced by the add-ons. At $\beta = 4°$ (Figure 9b), a similar increasing trend of power with tip speed ratio is observed, but the overall power values are significantly higher than those obtained at $\beta = -2°$. The maximum power reaches about 65 W at $\lambda = 0.50$, again with the

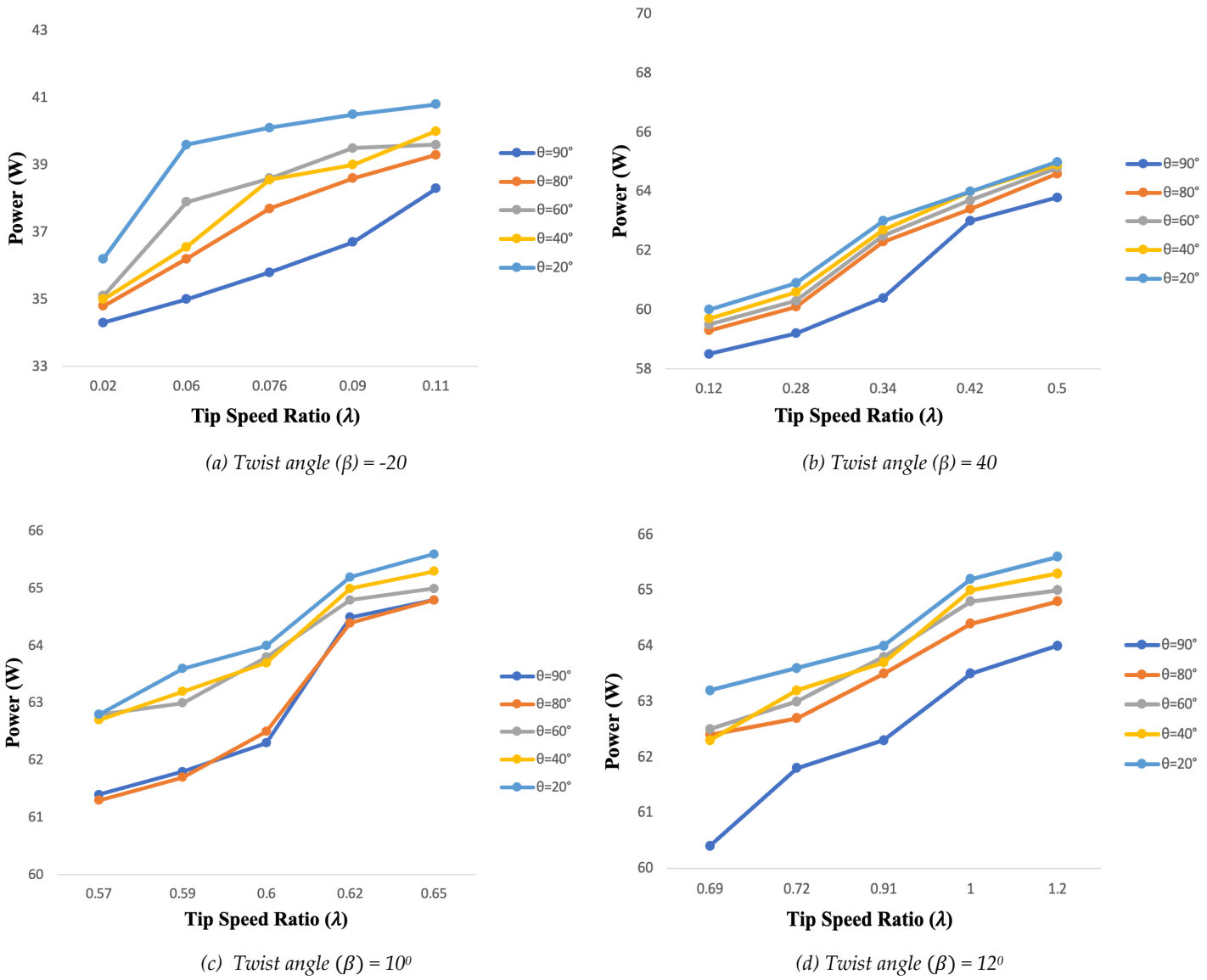

Figure 9. Effect of tip speed-ratio, cant-angle on power output of turbine at twist-angles.

θ = 20° case showing the best aerodynamic performance. The improvement at the higher twist angle indicates that blade twist strongly influences the effectiveness of winglet and spoiler add-ons by modifying the angle of attack distribution along the blade span. The combination of an appropriate twist angle with a favorable add-on orientation improves pressure distribution and strengthens the aerodynamic loading on the blade.

Comparing both twist conditions, the β = 4° configuration provides superior performance across all θ values, indicating that blade twist optimization works synergistically with winglet and spoiler modifications. The results therefore confirm that careful aerodynamic integration of blade twist and add-on geometry can significantly enhance HAWT power output, with θ = 20° emerging as the optimum orientation under the simulated conditions. This supports the CFD-based conclusion that winglet and spoiler add-ons can be effective passive flow-control devices for improving wind turbine blade efficiency when properly designed.

For β = 10° (Figure 9c), the power output increases steadily with tip speed ratio for all spoiler deflection angles, indicating improved aerodynamic efficiency as the rotor operates closer to its optimal TSR range. Among the configurations, θ = 20° consistently delivers the highest power output, reaching peak values of approximately 65–66 W at $\lambda \approx 0.65$. This trend reinforces earlier observations that small spoiler deflections enhance blade performance by promoting favorable pressure distribution and delaying boundary layer separation. Moderate deflections (θ = 40° and 60°) also perform competitively, while larger deflection (θ = 90°) results in comparatively lower power output, likely due to increased drag and flow disturbance. The smoother and more gradual rise in power suggests that at β = 10°, the blade operates under more stable aerodynamic conditions, benefiting from improved lift-to-drag characteristics.

For β = 12° (Figure 9d), a similar increasing trend with TSR is observed; however, the rate of improvement is slightly more gradual compared to β = 10°. Again, θ = 20°

produces the performance, achieving peak power values around 65.5–66 W at $\lambda \approx 1.2$. The higher twist angle shifts the optimal operating region to higher TSR values, indicating that the blade is better suited for faster rotational speeds. While performance gains are still evident with small spoiler angles, the relative difference between configurations becomes less pronounced at higher TSR, suggesting diminishing sensitivity to spoiler variation at very high twist angles. The $\theta = 90°$ case continues to underperform, confirming that excessive spoiler deflection introduces aerodynamic penalties such as increased wake losses and premature flow separation.

Comparatively, the results for $\beta = 10°$ and $\beta = 12°$ indicate that there exists an optimal twist–spoiler combination, beyond which further increases in twist angle do not yield proportional performance improvements. While $\beta = 12°$ extends the operational TSR range, $\beta = 10°$ appears to provide a more balanced enhancement in power output and aerodynamic stability.

4. Conclusion

This study has shown that aerodynamic add-ons, such as spoilers and winglets, can significantly improve the performance of a wind turbine blade by reducing aerodynamic losses and increasing power output. In this study, the numerical results of a horizontal axis wind turbine (HAWT) with an aerodynamic add-on were analyzed using the computational fluid dynamics (CFD) software COMSOL Multiphysics. The simulation results showed that the addition of the aerodynamic add-on can reduce the drag force and surface pressure coefficient on the blade, and improve the overall aerodynamic performance of the HAWT. The study presented a comprehensive parametric analysis of the winglet design, incorporating a meticulous assessment of the following parameters: winglet height (4% to 13% R), cant angle (20°, 40°, 60°, 80°, 90°), twist angle (-2°, 4°, 10°, 12°), and tip speed ratio (0.02 to 1.12) at a velocity of 3m/s. The incorporation of a winglet has effectively curbed the influence of wingtip vortices, which emerge due to the pressure differential between the upper and lower blade surfaces. A crucial finding of the study was the critical significance of the winglet's twist angle and cant angle in its design. The mechanical power diminishes as the cant angle is amplified, while the opposite trend is observed with the winglet height, which rises to a threshold beyond which the added height increases the induced drag, thereby decreasing the mechanical power. The study's results contribute to the ongoing efforts to enhance the efficiency of wind turbines and reduce their environmental impact. Additionally, the study is limited to a single wind turbine type and does not consider other factors such as wind speed, wind direction, or the impact of environmental conditions. Therefore, further research and testing are needed to validate the results and to determine the feasibility of using add-on devices in HAWT systems.

5. Nomenclature

ω	Angular Velocity
$\boldsymbol{C_P}$	Power of Coefficient
T	Torque.
A	Rotor of Swept Area
CFD	Computational Fluids Dynamics
HAWT	Horizontal Axis Wind Turbine
Re	Reynolds Number
$\boldsymbol{U_\infty}$	Wind Speed
$\boldsymbol{U_w}$	Velocity at the infinity wind turbine downstream
$\boldsymbol{U_d}$	Axial velocity of fluid passing through the wind rotor
$\boldsymbol{C_{pressure}}$	The pressure coefficient
$\boldsymbol{P}$	Static pressure
$\boldsymbol{P_\infty}$	Free-stream static pressure
$\boldsymbol{r}$	Radial distance from the hub Centre to the blade section
F_D	Drag Force
$\boldsymbol{\rho}$	Density of air
K	Tensor viscous effect
$\boldsymbol{\tau}$	Stress tensor
V	Velocity of the oncoming airstream
$\boldsymbol{\mu_t}$	Chord length
$\boldsymbol{\mu}$	Dynamic viscosity of air
∇	Differential operators are represented by a gradient
∇^2	Laplace Operator.

I	Identity matrix
F	External forces or sources
$\boldsymbol{\lambda}$	Tip Speed Ratio
u	Velocity vector of the fluid

6. Declarations

6.1. Author Contributions

Oluwaseyi Omotayo Alabi: Conceptualization, Methodology, Software, Validation, Formal analysis, Investigation, Resources, Formal analysis, Investigation, Resources, Data Curation, Writing - Original Draft; **Adeoti Oyegbori Laoye:** Formal analysis, Investigation, Resources, Data Curation, Writing - Original Draft; **Saidat Abisoye Salisu:** Writing - Review & Editing, Visualization, Supervision, Project administration, Funding acquisition.

6.2. Institutional Review Board Statement

Not applicable.

6.3. Informed Consent Statement

Not applicable.

6.4. Data Availability Statement

No data availability.

6.5. Acknowledgment

Not applicable.

6.6. Conflicts of Interest

The authors declare no conflicts of interest.

7. References

[1] K. A. Makinde, O. B. Adewuyi, A. O. Amole and O. A. Adeaga, "Design of Grid-connected and Stand-alone Photovoltaic Systems for Residential Energy Usage: A Technical Analysis," *Journal of Energy Research and Reviews.* vol. 8, no. 1, pp. 34-50, 2021. http://doi.org/10.9734/JENRR/2021/v8i130203.

[2] O. A. Adeaga, "Towards Numerical Investigation of Velocity Variation on Thin Ellipsoidal Aerofoil (NACA 3520) Using Surface Vorticity Method," *2023 Int. Conf. Sci. Eng. Bus. Sustain. Dev. Goals*, vol. 1, no. Naca 3520, pp. 1–8. https://doi.org/10.1109/SEB-SDG57117.2023.10124382.

[3] S. K. Ung, W. T. Chong, S. Mat, J. H. Ng, Y. H. Kok, and K. H. Wong, "Investigation into the Aerodynamic Performance of a Vertical Axis Wind Turbine with Endplate Design," *Energies*, vol. 15, no. 19, 2022. https://doi.org/10.3390/en15196925.

[4] O. O. Alabi, G. O. Ogunsiji, and S. A. Dada, "Performances evaluation of blended alternative refrigerant in vapour compression refrigeration system.," *Fed. Trend Sci. Technolojy Journal.*, vol. 8, no. 2, pp. 37–44, 2023. https://www.researchgate.net/profile/Samuel-Dada-6/publication/373683323.

[5] O. A. Adeaga, O.O. Alabi, S. A. Akintola, "Experimental Investigation of the Potential of Liquified Petroleum Gas in Vapour Compression Refrigeration System," *LAUTECH Journal of Engineering and Technology*, vol. 17, no. 1, pp. 1–7, 2023. https://www.laujet.com/index.php/laujet/article/view/544.

[6] Z. Li, M. Liu, X. Cao, M. Gao, L. Cheng, and H. Sun, "Aerodynamic performance analysis and power generation characteristics experiment of vertical axis wind turbine," *Eng. Reports*, vol. 4, no. 4, pp. 1–14, 2022. https://doi.org/10.1002/eng2.12500.

[7] B. Zhu, X. Sun, Y. Wang, and D. Huang, "Performance characteristics of a horizontal axis turbine with fusion winglet," *Energy*, vol. 120, pp. 431–440, 2017. https://doi.org/10.1016/j.energy.2016.11.094.

[8] O. A. Gaheen, M. A. Aziz, M. Hamza, H. Kashkoush, and M. A. Khalifa, "Fluid and Structure Analysis of Wind Turbine Blade with Winglet," *J. Adv. Res. Fluid Mech. Therm. Sci.*, vol. 90, no. 1, pp. 80–101, 2022. https://doi.org/10.37934/arfmts.90.1.80101.

[9] M. Sessarego, N. Ramos-Garcia, and W. Z. Shen, "Analysis of winglets and sweep on wind turbine blades using a lifting line vortex particle method in complex inflow conditions," *J. Phys. Conf. Ser.*, vol. 1037, no. 2, 2018. https://doi.org/10.1088/1742-6596/1037/2/022021.

[10] N. A. Satwika, R. Hantoro, S. Sarwono, and G. Nugroho, "Experimental investigation and numerical analysis on horizontal axis wind turbine with winglet and pitch variations," *Eng. J.*, vol. 23, no. 6, pp. 345–360, 2019. https://doi.org/10.4186/ej.2019.23.6.345.

[11] T. H. Hansen and F. Mühle, "Winglet optimization for a model-scale wind turbine," *Wind Energy*, vol. 21, no. 8, pp. 634–649, 2018. https://doi.org/10.1002/we.2183.

[12] L. Li, Y. H. Li, Q. K. Liu, and H. W. Lv, "A mathematical model for horizontal axis wind turbine blades," *Appl. Math. Model.*, vol. 38, no. 11–12, pp. 2695–2715, 2014. https://doi.org/10.1016/j.apm.2013.10.068.

[13] T. Khan, B. Singh, M. Thariq, H. Sultan, K. A. Ahmad, "Performance of a HAWT Rotor with a Modified Blade Configuration," *Pertanika J. Sci. & Technol*. vol. 30, no 1, pp. 201-220, 2021. https://doi.org/10.47836/pjst.30.1.11.

[14] A. Eltayesh *et al.*, "Experimental and numerical investigation of the effect of blade number on the aerodynamic performance of a small-scale horizontal axis wind turbine," *Alexandria Eng. J.*, vol. 60, no. 4, pp. 3931–3944, 2021. https://doi.org/10.1016/j.aej.2021.02.048.

[15] D. Gueraiche and S. Popov, "Winglet geometry impact on DLR-F4 aerodynamics and an analysis of a hyperbolic winglet concept," *Aerospace*, vol. 4, no. 4, 2017. https://doi.org/10.3390/aerospace4040060.

[16] M. H. A. Madsen, F. Zahle, S. G. Horcas, T. K. Barlas, and N. N. Sørensen, "CFD-based curved tip shape design for wind turbine blades," *Wind Energy Sci.*, vol. 7, no. 4, pp. 1471–1501, 2022. https://doi.org/10.5194/wes-7-1471-2022.

[17] M. G. Khalafallah, A. M. Ahmed, and M. K. Emam, "The effect of using winglets to enhance the performance of swept blades of a horizontal axis wind turbine," *Adv. Mech. Eng.*, vol. 11, no. 9, pp. 1–10, 2019. https://doi.org/10.1177/1687814019878312.

[18] M. G. Mourad, I. Shahin, S. S. Ayad, O. E. Abdellatif, and T. A. Mekhail, "Effect of winglet geometry on horizontal axis wind turbine performance," *Eng. Reports*, vol. 2, no. 1, pp. 1–19, 2020. https://doi.org/10.1002/eng2.12101.

[19] S. R. Reddy, G. S. Dulikravich, H. Sobieczky, and M. Gonzalez, "Bladelets-Winglets on Blades of Wind Turbines: A Multiobjective Design Optimization Study," *J. Sol. Energy Eng. Trans. ASME*, vol. 141, no. 6, 2019. https://doi.org/10.1115/1.4043657.

[20] N. A. Satwika, Sarwono, and R. Hantoro, "Investigation Flow on Horizontal Axis Wind Turbine with Betz Chord Distribution, Twist, and Winglet," *Proc. - 2018 4th Int. Conf. Sci. Technol. ICST 2018*, vol. 1, pp. 1–6, 2018. https://doi.org/10.1109/ICSTC.2018.8528653.

[21] S. Verma, A. R. Paul, A. Jain, and F. Alam, "Numerical investigation of stall characteristics for winglet blade of a horizontal axis wind turbine," *E3S Web Conf.*, vol. 321, 2021. https://doi.org/10.1051/e3sconf/202132103004.

[22] X. Hua, C. Zhang, J. Wei, X. Hu, and H. Wei, "Wind turbine bionic blade design and performance analysis," *J. Vis. Commun. Image Represent.*, vol. 60, pp. 258–265, 2019. https://doi.org/10.1016/j.jvcir.2019.01.037.

[23] S. Amroune *et al.*, "Manufacturing of Rapid Prototypes of Mechanical Parts Using Reverse Engineering and 3D Printing," *J. Serbian Soc. Comput. Mech.*, vol. 15, no. 1, pp. 167–176, 2021. https://doi.org/10.24874/jsscm.2021.15.01.11.

[24] S. Amroune, A. Belaadi, N. Menasri, M. Zaoui, B. Mohamad, and H. Amin, "New approach for computer-aided static balancing of turbines rotors," *Diagnostyka*, vol. 20, no. 4, pp. 95–101, 2019. https://doi.org/10.29354/diag/114621.

[25] S. Amroune, B. Mohamad, M. Moussaoui, and H. Saaidi, "Geometric regeneration and mechanical analysis of a gas turbine blade type frame 9001 GE," *Eng. Solid Mech.*, vol. 6, no. 2, pp. 105–112, 2018. https://doi.org/10.5267/j.esm.2018.3.003.

[26] H. M. S. M. Mazarbhuiya, A. Biswas, and K. K. Sharma, "A 2D numerical simulation of blade twist effect on the aerodynamic performance of an asymmetric blade vertical axis wind turbine in low wind speed," *EAI Endorsed Trans. Energy Web*, vol. 7, no. 28, pp. 1–7, 2020. https://doi.org/10.4108/EAI.13-7-2018.162828.

[27] O. Erkan, M. Özkan, T. H. Karakoç, S. J. Garrett, and P. J. Thomas, "Investigation of aerodynamic performance characteristics of a wind-turbine-blade profile using the finite-volume method," *Renew. Energy*, vol. m, 2020. https://doi.org/10.1016/j.renene.2020.07.138.

[28] O. O. Alabi, O. A. Adeaga, and S. A. Akintola, "Numerical Modeling and Investigation of Flow of Incompressible Non-Newtonian Fluids through Uniform Slightly Deformable Channel," *2023 Int. Conf. Sci. Eng. Bus. Sustain. Dev. Goals*, vol. 1, no. 1984, pp. 1–6, 2020. https://doi.org/10.1109/SEB-SDG57117.2023.10124471.